HHS Public Access

Author manuscript

*Biochemistry*. Author manuscript; available in PMC 2017 May 17.

Published in final edited form as:

*Biochemistry*. 2016 May 17; 55(19): 2760–2771. doi:10.1021/acs.biochem.6b00181.

# Structural and Kinetic Studies of Formate Dehydrogenase from *Candida boidinii*

**Qi Guo**[1], **Lokesh Gakhar**[2], **Kyle Wickersham**[1], **Kevin Francis**[1], **Alexandra Vardi-Kilshtain**[3], **Dan T. Major**[3], **Christopher M. Cheatum**[1], and **Amnon Kohen**[1,*]

[1]Department of Chemistry, University of Iowa, Iowa City, IA 52242, United States

[2]Protein Crystallography Facility and Department of Biochemistry, University of Iowa, Iowa City, IA 52242, United States

[3]Department of Chemistry and the Lise Meitner-Minerva Center of Computational Quantum Chemistry, Bar-Ilan University, Ramat-Gan 5290002, Israel

## Abstract

The structure of formate dehydrogenase from *Candida boidinii* (CbFDH) is of both academic and practical interests. First, this enzyme represents a unique model system in studies of the role of protein dynamics in catalysis, but so far these studies were limited by the availability of structural information. Second, CbFDH and its mutants are of use in various industrial applications (e.g., $CO_2$ fixation or nicotinamide recycling systems), and the lack of structural information has been a limiting factor in its commercial development. Here, we report the crystallization and structural determination of both holo-CbFDH and apo-CbFDH. The free energy barrier for the catalyzed reaction is computed, and indicates that this structure indeed represents a catalytically competent form of the enzyme. Complementing kinetic examinations demonstrate that the recombinant CbFDH has a well-organized reactive state. Finally, a fortuitous observation has been made: The apo-enzyme crystal was obtained under co-crystallization conditions with a saturating concentration of both the cofactor ($NAD^+$) and inhibitor (azide), which has a nM dissociation constant. It was found that the fraction of the apo-enzyme present in the solution is less than $1.7x10^{-7}$ (i.e. the solution is 99.9999% holo-enzyme). This is an extreme case where the crystal structure represents an insignificant fraction of enzyme in solution, and a mechanism rationalizing this phenomenon is presented.

*To whom correspondence may be addressed. Professor Amnon Kohen, Department of Chemistry, The University of Iowa, Iowa City, IA 52242, U.S.A. Tel.: +1 319 335 0234; amnon-kohen@uiowa.edu.

**AUTHOR CONTRIBUTIONS**

AK and CMC coordinated the project. QG designed and performed the bulk of experiments. LG assisted in the X-ray data collection and refinement. KW was involved in the protein preparation and characterization. KF assisted the pre-steady state kinetics studies. AV-K and DTM performed the QM/MM calculations. QG and AK wrote the manuscript and all authors reviewed it before submission.

**CONFLICT OF INTEREST**

The authors declare that they have no conflicts of interest with the contents of this article.

SUPPORTING INFORMATION AVALIBLE

Tables showing the observed and intrinsic H/T and D/T KIEs, crystallization data collection and refinement and comparison of ensemble averaged distances (Å) from MD simulations of the ground state in PsFDH and CbFDH are provided. In addition, figures showing the IEF and MALDI-TOF characterization on commercial and recombinant CbFDH are shown. Also available is a movie presenting the motions needed when the apo-enzyme (open conformation) binds the substrates and rearranges to the reactive complex (closed conformation). This information is available free of charge via the Internet at http://pubs.acs.org/.

## Graphical Abstract

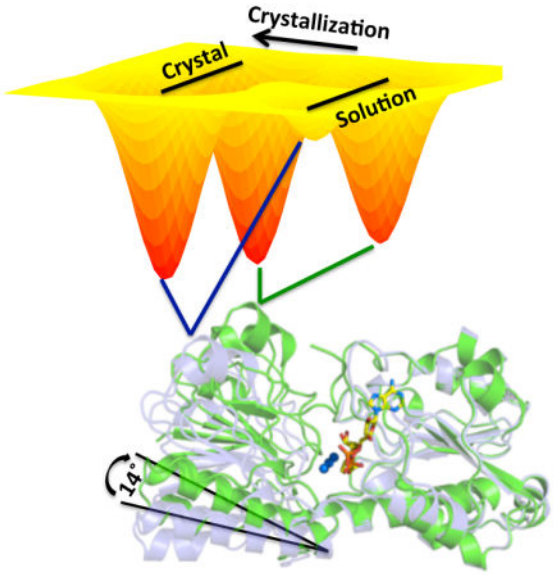


### Keywords

formate dehydrogenase; crystal structure; enzyme kinetics; isotope effects; QM/MM calculations

Formate dehydrogenase (FDH, EC 1.2.1.2) is a homodimer with two independent active sites[1] catalyzing the $NAD^+$-dependent oxidation of formate to $CO_2$ (Scheme 1)[2–4] via an irreversible hydride transfer from formate to $NAD^+$.[5]

Formate dehydrogenase from *Candida boidinii* (CbFDH) is an attractive system for correlating kinetics and dynamics since the nature of its chemical step can be probed,[2] and its transition state analog (TSA), azide, is both a tight inhibitor ($K_I$=40 nM) and a good IR probe – enabling vibrational spectroscopy studies of the dynamics in an excellent mimic of the activated complex. Azide is a TSA because it is isoelectronic with the carbon dioxide product and negatively charged like the formate anion reactant (Scheme 1).[5] In addition, azide is a strong vibrational chromophore with a characteristic IR absorption at ~2045 $cm^{-1}$ that is separated from the absorptions of other functional groups in an enzyme-solvent system.[7] Two-dimensional infrared (2D IR) spectroscopy can assess the femtosecond (fs) to picosecond (ps) motions of the active site of a reactive-like complex (FDH-$NAD^+$-azide) by probing the frequency fluctuations of the antisymmetric stretch of the azide anion.[8–11] Characterizing both the kinetics of the chemical step and the active site dynamics will require structure-guided mutagenesis of active-site residues.[12–14] In the past, a commercially available CbFDH has been used to characterize the nature of the H-transfer and the active site dynamics.[2,10,11] As in the case of most wild type enzymes, those studies found temperature independent intrinsic kinetic isotope effects (KIEs),[2] which indicate that the donor-acceptor distance (DAD) at the tunneling ready state (TRS) is narrowly distributed (well organized) for H-tunneling.[15] However, the fact that the commercial enzyme was a

mixture of isozymes (see below) and the lack of a crystal structure of its TSA complex prohibited further investigation of that system.

Mechanistic studies of most enzymes involve site-directed mutagenesis or other methods that require the use of a recombinant enzyme and knowledge of its structure in a reactive conformation (e.g., mimicked by complex with the TSA, azide, and $NAD^+$ in the case of FDH). So far, the only crystal structure of FDH in ternary complex was for the enzyme from *Pseudomonas* sp.101 (PsFDH, PDB ID 2NAD),[4] and computational studies based on this structure demonstrated dynamic effects of protein motions in FDH system.[16–19] However, direct measurements of dynamic effects were revealed in the case of CbFDH,[6,10,11] therefore using a homology-model from PsFDH ternary complex limited commercial and basic applications for both experimental designs and computations.[6,10,11,18] The only two crystal structures available for CbFDH are for the apo-enzyme and each includes a single-point mutant (K47E, PDB 2FSS and K328V, PDB 2J6I) designed via an adapted surface engineering approach.[20] Even if those mutants do represent the wild type structure, structures of apo-CbFDH provide limited guidelines for mutagenesis studies and high level computations, which necessitates the X-ray structure of the ternary complex in its reactive form.

In addition to the importance of obtaining the structure of CbFDH for mechanistic studies, detailed structural exploration would assist CbFDH engineering for industrial applications. Industrial technologies for obtaining large quantities of FDH from *Candida boidinii* have long been described,[21] and FDHs have been extensively studied as a candidate for developing industrial NAD(P)H[22–24] regeneration and $CO_2$ consumption systems.[25]

The current work describes the design, expression, and purification of recombinant CbFDH, followed by the determination of structures of co-crystallized CbFDH with $NAD^+$ and azide, as well as the apo-enzyme. The apo- and holo-structures were solved to a resolution of 1.75 and 1.5 Å, and were assigned PDB IDs 5DNA and 5DN9, respectively when deposited into Protein Data Bank. The kinetic features of the recombinant CbFDH were also examined and compared with the commercial enzyme (a mixture of isozymes). Finally, to probe the catalytic competency of the holo-structure, quantum mechanical/molecular mechanical (QM/MM) simulations were carried out to obtain the reaction free energy profile for CbFDH and this profile was compared to that of PsFDH.

## MATERIALS AND METHODS

### Materials

The pET-23a plasmid harboring the gene encoding for CbFDH was a generous gift from Dr. Nikolaos Labrou of the Agricultural University of Athens. *E. coli* BL21 (DE3) pLysS cells were from Novagen. Blue sepharose 6 fast flow and Superdex 200 resin were from GE Healthcare Life Sciences. Bradford dye reagent, immobilized pH gradient (IPG) strips for isoelectric focusing (IEF), SDS gels and the protein standards were from Bio-Rad. [Ad-$^{14}$C]-$NAD^+$ was from PerkinElmer. [$^3$H]-formic acid was from Moravek Biochemicals. All other materials were purchased from Sigma-Aldrich unless otherwise specified.

### Expression and purification of CbFDH

CbFDH plasmids were transformed into BL21 (DE3) pLysS cells and grown in 6 L Luria-Bertani medium with 100 mg/L ampicillin at 37°C and 250 rpm. Expression of CbFDH was induced by the addition of 1 mM of isopropyl β-D-1-thiogalactopyranoside (IPTG) when the $OD_{600}$ reached ~0.6. The cells were incubated overnight and harvested by centrifugation at 5,000 g for 30 min at 4 °C. The cell paste (~25 g) was then suspended in lysis buffer (50 mM potassium phosphate, 5 mM EDTA, 10% glycerol, pH 7.5) for 1 hr and lysed by French pressing, and then centrifuged at 10,000 g for 1 hr. The supernatant was dialyzed overnight at 4°C against 100-vol. of 10 mM MES/NaOH buffer, pH 6.0 followed by another centrifugation at 10,000 g for 1 hr. Then the supernatant was clarified by filtration through a Millipore cellulose membrane filter (0.22 μm pore size). The filtered solution was purified by affinity chromatography using Blue Sepharose 6 fast flow resin following the procedure described previously.[26,27] The enzyme was purified to a high level as judged by SDS-PAGE, and then dialyzed against 100 mM potassium phosphate pH 7.5 and stored at −80 °C.

### Steady-state kinetics

The $K_{M/NAD^+}$ and $k_{cat}$ were determined through initial velocity studies varying the $NAD^+$ concentration from 0.02 to 12 mM at a formate concentration of 200 mM. The production of NADH was monitored by following UV absorption at 340 nm in 100 mM phosphate buffer at pH 7.5 and 25°C. The reaction was initiated by adding 0.2 μM CbFDH (final concentration). Similarly, $K_{M/formate}$ was measured under the same buffer and enzyme concentration by varying the formate concentration from 1 to 215 mM at a $NAD^+$ concentration of 10 mM. Data were fit to the Michaelis–Menten equation to obtain the kinetic parameters $k_{cat}$ and $K_M$ for both substrates.

### Crystallization of CbFDH

Prior to preparation of ternary complexes for crystallization, the protein was freshly purified by affinity chromatography (Blue Sepharose 6), and a Superdex-200 gel filtration column that was pre-equilibrated with 20 mM bis-tris-propane buffer containing 150 mM NaCl, pH 7.8.[20] The protein was then concentrated and the concentration was determined using the Bradford assay. $NAD^+$ and sodium azide at 50-fold molar excess relative to the concentration of CbFDH were then added and the mixture was incubated on ice for at least 1 h. The monodispersity of the concentrated CbFDH in complex with $NAD^+$ and azide was tested using dynamic light scattering (DLS) on a NanoStar instrument (Wyatt Technology). Both apo- and holo-structures were crystallized via the hanging-drop vapor diffusion method at 18°C with the drop containing 0.4 μl of both CbFDH-$NAD^+$-azide ternary complex and crystallization solutions using TTP LabTech Mosquito.

### Data collection and structure determination

Crystals were flash-cooled in liquid nitrogen. Data of the apo-CbFDH were collected at 100 K via the in-house Rigaku diffractometer at the Protein Crystallography Facility, University of Iowa. Data for holo-CbFDH were collected at the 4.2.2 synchrotron beamline at the Advanced Light Source (Berkeley, CA, USA). The data were processed using XDS.[28] The structure of CbFDH K328V mutant (PDB 2J6I)[20] was used as a template for molecular

replacement (MR). For the closed conformation holo-CbFDH, the 2J6I structure was broken down to domain A (residues 117–313) and domain B (residues 1–115 and 315–361), and used as MR templates. MR was performed using the program PHASER,[29] which is part of the CCP4 software suite.[30] Model building was performed in Coot.[31] Further refinement was carried out using REFMAC5[32] and Phenix.[33]

## Isothermal titration calorimetry (ITC)

ITC experiments were performed using MicroCal iTC200 (GE Healthcare). To determine whether buffer conditions affect ligand binding, we performed the same ITC measurements in either 100 mM phosphate, pH 7.5 or 10 mM bis-tris-propane, 0.05 M HEPES buffer containing 75 mM NaCl and 0.05 M sodium acetate trihydrate, 12% PEG 4000, pH 7.5. The latter is the crystallization condition under which apo-enzyme crystals were obtained. Before ITC experiments, FDH was dialyzed against the buffer overnight and then concentrated. The same dialysis buffer was used to make $NAD^+$ or sodium azide solutions. When measuring the binding constant of $NAD^+$ to FDH, a sample cell containing 50 μM FDH (active site) was titrated with 2 mM $NAD^+$. To measure the binding constant of azide to FDH-$NAD^+$ complex, a sample cell containing 20 μM FDH mixed with 1mM $NAD^+$, and was titrated with 1 mM azide. The temperature of the calorimeter cells (sample and reference) was maintained at 25 °C. The data obtained were fit using one-set models Origin 7 (provided with the instrument).

## Kinetic isotope effect measurements

Both H/T and D/T competitive KIEs were measured to determine the intrinsic KIEs for CbFDH at 5, 15, 25, 35 and 45 °C following the procedure described in ref [6]. Briefly, in 1 ml final volume of 100 mM phosphate buffer (pH 7.5), trace amounts of [Ad-$^{14}$C]-$NAD^+$ (660,000 dpm) and [$^3$H]-formic acid (3,300,000 dpm) were mixed with 50 mM $NAD^+$ and 40 mM formic acid (for H/T) or 99.8% deuterated formic acid (for D/T). During the reaction, the hydride or deuteride is transferred from formic acid to [Ad-$^{14}$C]-$NAD^+$ to form [Ad-$^{14}$C]-NADH/D. Similarly, [$^3$H]-NADH is also produced from [$^3$H]-formic acid. Therefore, [Ad-$^{14}$C]-NADH/D represents the protium or deuterium transferred, and [$^3$H]-NADH represents the tritium transferred. The reaction was initiated by adding CbFDH, and 100 μl aliquots are removed at various fraction conversions and quenched by adding 20 μl of 50 mM azide. All samples were immediately frozen on dry ice and then kept at −80 °C until analyzed on the HPLC. The HPLC separation was followed by liquid scintillation counter (LSC) analysis to determine the depletion of $^3$H relative to $^{14}$C in the product at different fractional conversions. The observed KIEs were calculated using eq. (1)

$$KIE = \frac{\ln(1-f)}{\ln[1-f(R_t/R_\infty)]} \quad (1)$$

where $f$ is the fractional conversion based on $^{14}$C-$NAD^+$ and $R_t$ and $R_\infty$ are the isotope ratios between $^3$H and $^{14}$C at time t and infinity, respectively:

$$f = \frac{[^{14}C]NADH}{(100 - \%excess)([^{14}C]NADH + [^{14}C]NAD^{+})} \quad (2)$$

$$R = \frac{^{3}H_{NADH}}{^{14}C_{NADH}} \quad (3)$$

Intrinsic KIEs were calculated from their observed values using a numerical solution of the modified Northrop equation:[34,35]

$$\frac{^{T}(V/K)^{-1}_{Hobs} - 1}{^{T}(V/K)^{-1}_{Dobs} - 1} = \frac{(k_H/k_T)^{-1} - 1}{(k_H/k_T)^{-1/3.3} - 1} \quad (4)$$

where $k_H/k_T$ is the intrinsic H/T KIE and $^{T}(V/K)_{H,obs}$ and $^{T}(V/K)_{D,obs}$ are the observed H/T and D/T KIE values for the second-order rate constant $k_{cat}/K_M$, respectively.

## Pre-steady-state kinetics

The single turnover rate of both recombinant and commercial CbFDH were measured in 100 mM potassium phosphate, pH 7.5 by following the production of NADH at 340 nm using an Applied Photophysics stopped-flow spectrophotometer maintained at 25 °C. 84 μM CbFDH (concentration of active sites) was pre-incubated with 62 μM $NAD^+$ and the reaction was initiated by mixing with an equal volume of sodium formate (40 mM) in the same buffer. The kinetic traces were fit to a single exponential function to obtain the single turnover rates.

## QM/MM calculation

The crystal structures of holo-PsFDH (PDB 2NAD)[4] and of holo-CbFDH (PDB 5DN9) were used to construct the initial configuration for the present study. The setup and the MD simulations of all systems were carried out based on procedures similar to those employed for the wild type PsFDH.[18] Briefly, the protonation states of all polar amino acid residue side chains were adjusted to pH 7, and the protonation states of the His residues were determined so as to match the hydrogen bonding patterns in the nearest environment. The HBUILD facility in the program CHARMM was applied to add hydrogen atoms. Sodium ions were added to the wild type systems (14 for PsFDH and 2 for CbFDH) to neutralize the overall negative charge.

The potential energy surface in the current study is described by a hybrid QM/MM Hamiltonian,[36] where the QM region is treated by a modified AM1[37] semiempirical Hamiltonian, denoted AM1-SRP (specific reaction parameters). [18,38]

The QM region includes the fragments NADH and $CO_2$, which are proximal to the reaction center, whereas the MM region contains the remaining ligand atoms, the entire protein,

water molecules and sodium ions. The water molecules were represented by the three-point charge TIP3P model.[39] Hydrogen link atoms were placed across the bonds intersected by the QM/MM boundary, and the QM/MM interactions were treated using electrostatic embedding. A detailed QM/MM partitioning scheme and a thorough description of the development of the AM1-SRP Hamiltonian for FDH is provided elsewhere.[18] In modeling the MM region, we used the all-atom CHARMM22 force field.[40]

Periodic boundary conditions were employed to solvate the Michaelis complex using a pre-equilibrated cubic water box (PsFDH system: ~92 Å × ~92 Å × ~92 Å; CbFDH system ~97 Å × ~97 Å × ~97 Å), while treating long-range electrostatic interactions with the Ewald summation technique (90 × 90 × 90 FFT grid for PsFDH system and 96 × 96 × 96 for the CbFDH system, $\varkappa$; = 0.340 $Å^{-1}$).[41] The PsFDH and CbFDH systems were fully minimized, and heated up gradually to 298 K for 25 ps. Both systems were equilibrated at that temperature for 1 ns at the MM level of theory. Each system was thereafter re-equilibrated using the QM(AM1-SRP)/MM potential over the course of 200 ps. All equilibrations and subsequent simulations were conducted with the isothermal-isobaric (*NPT*) ensemble at 1 atm and at the target temperature. The pressure and temperature were controlled by the extended constant pressure/temperature (CPT) method[42] and the Hoover thermostat,[43] respectively. The leapfrog integration scheme[44] was used to propagate the equations of motion, and the SHAKE algorithm[45] was applied to constrain all MM bonds involving hydrogen atoms, allowing a time step of 1 fs. During the equilibration, several nuclear Overhauser effect (NOE) restraints were imposed on key hydrogen bond interactions between the ligands and the surrounding residues, and removed 200 ps before moving on to the production phase. All enzyme simulations used a development version of the CHARMM program.[46,47] Complementary details of the MD simulations are available in our earlier work.[18]

The umbrella sampling (US) technique[48] was used to determine the classical-mechanical potential of mean force (CM-PMF) for the hydride transfer reaction. The reaction coordinate was defined as the antisymmetric reactive stretch coordinate, $\zeta_{asym}$, namely the difference between the lengths of the breaking C–H and forming H–C4N bonds. A total of 14 individual US MD simulations ("windows") were performed along discrete, evenly spaced values of from $\zeta_{asym}$ − 1.75 to 1.5 Å. Each window was subject to an appropriate harmonic restraint, which keeps $\zeta_{asym}$ in the desired region, and an umbrella potential (roughly the negative of the PMF) as a function of $\zeta_{asym}$. In order to efficiently update the biasing potential as necessary, each window was sampled in multiple successive series with a predetermined number of MD steps. A typical simulation starts with a short equilibration (2 ps), followed by collection of the probability densities of configurations ($\rho$) along the reaction coordinate, $\zeta_{asym}$. Whenever the biasing potential is updated, the subsequent simulation commences with a short equilibration, and the accompanying equilibration data is discarded. The cumulative simulation time per window was 375–400 ps. The statistics for all coordinates was sorted into bins of width 0.01 Å. The positions and velocities of the last recorded configuration in a specific window were used to start its successor, to maintain continuity of propagation. CM-PMF curves and surfaces were computed using a multidimensional version of the weighted histogram analysis method (WHAM).[49] QM PMFs were obtained by PI-US simulations as described in our earlier work.[18]

## RESULTS AND DISCUSSION

***Sequence alignment*** of the recombinant CbFDH with the surface mutant K328V and PsFDH are summarized in Figure 1. Schirwitz *et al.* concluded that it was difficult to crystallize the wild type CbFDH due to the many flexible loop regions, and two single-point surface mutations K328V and K47E were introduced to obtain the three dimensional structures for CbFDH (apo-form).[20] The two mutants (K328V and K47E) possess very similar kinetic and structural properties, so the comparison in this paper will only consider the K328V. The published K328V mutant was also different than the wild-type enzyme used here by three hydrophobic, but nonconserved variants: L128V, I227V and I354G (highlighted with * in Figure 1). The isoform of CbFDH used in ref [20] (CbFDH_iso1 in Figure 1) and the one used in this work (CbFDH_iso2) were directly cloned from yeast, and thus represented natural CbFDH isozymes, which accords with the various isozymes found in the commercial CbFDH (Figure S1). In this work, we did not need to introduce the artificial mutation K328V to get the enzyme to crystallize, suggesting that the currently used isozyme is more suitable for crystallization than the wild-type enzyme attempted in ref [20]. In addition, the commercial CbFDH did not crystallize, and it turned out to be a mixture of isozymes, as was confirmed by isoelectric focusing and matrix-assisted laser desorption/ionization-time of flight (MALDI-TOF) mass spectrometry analysis (Figure S1).

***The steady state kinetic parameters*** of recombinant CbFDH were measured and compared to those of the surface mutant K328V, the commercial CbFDH and PsFDH (Table 1). The steady-state kinetic parameters for the recombinant CbFDH and its surface mutant K328V are very similar. The commercial CbFDH has higher $K_{M/formate}$ and lower $k_{cat}/K_{M/formate}$ value, in accordance with a weighted average for its isozyme mixture that does not bind and capture the substrate as well as the recombinant isoform.

### X-ray structure

To study the role of active site protein dynamics close to the transition state of the FDH catalyzed reaction it is critical to choose relevant mutations based on the structure of the ternary (TS-like) complex of the enzyme under study. The co-crystallization conditions were set to assure formation of CbFDH all pre-bound to both ligands ($NAD^+$ and azide). However, along with crystals of that ternary complex, crystals of the apo-CbFDH were also obtained. This finding is quite astonishing requiring a more in depth examination (*vide infra*).

The apo-CbFDH crystallizes in the *P*1 space group under the crystallization conditions: 0.1 M sodium acetate trihydrate, 0.1 M HEPES, 25% PEG 4000, pH 7.5 within 10 days. The holo-FDH (Figure 2) crystallizes in the $P1\ 2_1\ 1$ space group under the conditions: 0.1 M HEPES, 25% PEG 3000, pH 7.5 within 15 days. Detailed X-ray data are summarized in Table S2. The protein solutions for both contained $NAD^+$ and sodium azide at 50-fold molar excess relative to the concentration of CbFDH. The initial concentration at which the apo-enzyme crystallized was 4.1 mg/ml (~0.1 mM active sites), while for the holo-enzyme it was 6 mg/ml (~0.15 mM active sites).

To assess the fraction of free enzyme under the apo-CbFDH crystallization condition, we used ITC to measure the $K_d$ for $NAD^+$ to CbFDH and azide to CbFDH-$NAD^+$ in buffer containing 0.1 M sodium acetate trihydrate, 0.1 M HEPES, 25% PEG 4000, pH 7.5, and the values are 92 ± 4 μM and 43 ± 5 nM, respectively. Equation (7) gives an effective dissociation equilibrium constant for the ternary complex that is derived by multiplying equations (5) and (6) for the individual binary equilibria. The crystallization solution that yielded apo-CbFDH crystals contained 0.1 mM CbFDH (active sites concentration) and 5 mM $NAD^+$ and azide. Using these concentrations in Eq. 7, leads to a ratio of free enzyme to ternary complex [E]/[E-$NAD^+$-azide] of $1.7x10^{-7}$; namely only 0.00001% of free enzyme in solution.

$$K_{d/NAD+} = 92\,\mu M = \frac{[E][NAD^+]}{[E-NAD^+]} \quad (5)$$

$$K_{d/N_3^-} = 43\,nM = \frac{[E][N_3^-]}{[E-N_3^-]} \quad (6)$$

$$K_{d/NAD^+N_3^-} = K_{d/NAD+} \cdot K_{d/N_3^-} = 4.0 \cdot 10^{-12}\,M^2 = \frac{[E][NAD^+][N_3^-]}{[E-NAD^+-N_3^-]} \quad (7)$$

Given such a low fraction of free enzyme in solution, it is quite remarkable that the apo- rather than the holo-enzyme crystalized. The relationship between the structure observed in the crystal and the dominant structure in solution has been examined since the beginning of protein crystallography. It is also known that crystal packing interactions can impede ligand binding,[52] and that poor reproducibility of structures crystalized under the same conditions can occur.[53] However, to the best of our knowledge, there have been no reports of similar observations where ligand-free protein crystallized while in solution more than 99.9999% is ligand-bound. We attribute most of this finding to the catalytic effect of nucleation centers that change the crystallization kinetics. A possible energy landscape that could explain this phenomenon is illustrated in Figure 3.

In this model, most of the enzyme in solution is ligand-bound (specie **c** in Figure 3), and has a much lower potential energy than the unbound enzymes in solution (specie **d**). Figure 3A illustrates a condition where nucleation lowers the free energy barrier for holo-enzyme crystallization, and Figure 3B illustrates the condition where the crystallization barrier is lowered for the apo-enzyme. The formation of these nucleation sites is catalytic for either path. The scenario presented in panel A is the expected one (99.9999% holo-enzyme). However, the very small population of unbound enzyme can also form a nucleation site that would initiate crystallization toward species **a** (the apo-enzyme), as illustrated in panel B. While we do not know whether the thermodynamics in the crystalline form favor ternary complex (state **b**) or apo-enzyme (state **a**) conformation, we know that under the crystallization conditions both are favored relative to the enzyme in solution. Furthermore,

the two crystalized forms cannot exchange without going back to solution (high barrier between **a** and **b**) being crystallized into very different crystals (different space groups, Table S2; and different packing, Figure 4). Thus although thermodynamically in solution only 0.000017% enzyme is free, the kinetic competition can still favor the formation of crystals of the apo-enzyme, and the thermodynamic driving force would lead to formation of only those crystals (Figure 3B).

Figure 4A shows the apo-CbFDH packing between chain A (blue) and chain D from a neighbouring cell unit (yellow). The black circled region highlights the conformation of the active site cleft that matches well with the neighbouring unit. In Figure 4B, the same asymmetric unit chain A of the holo-CbFDH (green) has a very different interface with chain D of the neighbouring cell unit (yellow). For the apo-enzyme it appears that the packing pattern prevented enzymes from forming the closed conformation. For the apo-CbFDH structure, these packing interactions appear to stabilize the open conformation and prevent conversion of one crystal structure to the other, in accordance with the high energy barrier between states **a** and **b** in Figure 3.

In Figure 5 the apo-enzyme is compared to the holo-enzyme, and the red arrows mark the needed motion from one to the other. This motion that follows the ligand binding is further emphasized in the movie enclosed in the SI. The apo-form has an open-conformation with a wide active site cleft, while the holo-form is in a closed-conformation. In the holo-form the complete catalytic domain is tilted inward by about 14°, thus narrowing the active site groove and closing the active site cleft.

## Kinetic isotope effects

As for most wild type enzymes with their natural substrates, studies of commercial CbFDH found temperature independent intrinsic KIEs.[2] The isotope effect on the pre-exponential Arrhenius factor $A_H/A_T = 6.1\pm0.5$ and the slope was zero within experimental error ($\Delta E_{aT\text{-}H} = -0.02\pm0.05$ kcal/mol). These findings invoked interest in CbFDH for examination of the enzyme-dynamics-function relations, but as discussed above, the commercial mixture of isoforms was not useful for either crystallization or mutational studies. The current studies of recombinant CbFDH also found temperature independent intrinsic KIEs (Figure 6). Both the observed and intrinsic KIEs are slightly inflated relative to the commercial mixture of isozymes (Table S1), with the pre-exponential factor $A_H/A_T = 6.8\pm2.0$, but it is as temperature independent as the mixture ($\Delta E_{aT\text{-}H} = 0.01\pm0.2$ kcal/mol).

The temperature independence of KIEs is interpreted as a well-organized donor-acceptor distance (DAD) for the H-transfer, and an optimal "fine-tuning" of the transition state (or the tunneling ready state) for the H-transfer step.[2,12,54–59] The inflated KIEs in the recombinant CbFDH reflect a longer average DAD than the average DAD in the commercial mixture.[60] Importantly, both systems have temperature independent intrinsic KIEs, indicating that the DAD is narrowly distributed in both the recombinant enzyme and the isozyme mixture as isolated from yeast – validating the use of the recombinant enzyme and its prospective mutants in biophysical studies similar to those of other enzymes (e.g., dihydrofolate reductase;[12,59,61] soybean lipoxygenase;[13,62,63] alcohol dehydrogenase;[14,64,65] and others).

## Pre-steady state kinetics

Single turnover reaction conditions were identical for both the recombinant and commercial CbFDHs (see experimental section). The data for recombinant CbFDH could be fitted with a single-exponential decay giving a single turnover rate ($k_{obs}$) of 35 ± 2 $s^{-1}$, with an amplitude consistent with consumption of all the pre-bound $NAD^+$ during a single turnover. The commercial enzyme, on the other hand, only consumed about ~30 % of the $NAD^+$ during the first turnover (~0.1 s), and was fit by a single-exponential followed by a linear steady-state phase (burst equation), giving presteady state $k_{obs}$ of 25 ± 4 $s^{-1}$ and steady state rate of 0.10 ± 0.02 $s^{-1}$. Both recombinant and commercial CbFDH showed a lag phase for the first 30 ms (Figure 7), which was not included in the regression.

The burst kinetics observed for the commercial CbFDH are consistent with the higher $K_M$ observed for $NAD^+$ (Table 1). Only 30 % of the $NAD^+$ was bound to the enzyme under the pre-incubation conditions, as is evident from the NADH fraction formed during the exponential phase of the reaction. The rest of the $NAD^+$ was consumed under steady-state conditions at the linear phase of the burst experiment (Figure 7B). The 30 ms lag phase may suggest that after binding formate the ternary complex undergoes a conformational change before reaching the reactive conformation for hydride transfer. Attempts to crystallize the CbFDH with $NAD^+$ alone (if successful) could test that hypothesis (the CbFDH-$NAD^+$ binary complex showing an open conformation would imply that after substrate binding, a major conformational change is necessary to reach the reactive conformation). Similar lag phases have been observed for other enzymatic systems[13,62,63] and while they all suggested some sort of delay in enzyme activation following the mixing with the second substrate, the lag-mechanism has not be mechanistically resolved.

## QM/MM calculation

To probe whether the holo-enzyme crystal structures of PsFDH and CbFDH both represent equally catalytically competent structures, we compared the catalytic reaction coordinate using the new structure of CbFDH-$NAD^+$-$N_3$ (PDB 5DN9) and that of the same complex with PsFDH (PDB 2NAD). We note that several studies have shown that different crystal structures can results in rather different simulated kinetics.[66,67] Figure 8 shows the classical mechanical potential of mean force (CM-PMF) for the wild-type PsFDH and CbFDH hydride transfer reaction obtained from free energy MD simulations, using the AM1-SRP QM/MM Hamiltonian. The free energy barrier predicted by the corresponding PMF for CbFDH is 14.2 kcal/mol, which is very similar to the value obtained for PsFDH ($\Delta G^{\ddagger}$ = 14.9 kcal/mol). The free energies of reaction for PsFDH (−10.8 kcal/mol) and CbFDH (−12.3 kcal/mol) are also fairly similar (Table 2).

The QM-PMF is obtained from Feynman path-integral calculations, in which the centroid positions of the discrete paths of quantized particles are used to specify the reaction coordinate.[68–70] Using QM(AM1-SRP)/MM, inclusion of NQE in the simulations[68] lowers the computed free energies of activation for the hydride by 1.9 kcal for PsFDH (13.0 kcal/mol)[18] and 2.0 kcal/mol for CbFDH (12.2 kcal/mol). The calculated free energy of activation is lower than that measured experimentally (16.6 kcal/mol),[4,71] which reflects the fact that the calculation corresponds exclusively to the hydride transfer step rather than

reflecting a phenomenological complex multistep rate constant. The intrinsic rate of the formate oxidation reaction computed herein is masked by other non-chemical kinetic steps, which contribute individually to the overall rate constant, as pointed out by Moliner and co-workers.[16] This fact is also in accordance with a smaller observed H/T KIE on $k_{cat}/K_M$ than its intrinsic value (Table S1), although this comparison is indirect as the reported barrier[4,71] is on the first order rate ($k_{cat}$), not the second order rate $k_{cat}/K_M$.

Comparison of ensemble averaged distances (Å) from MD simulations of the ground state in PsFDH and CbFDH is shown in Table S3. Analysis of the distances shows similar contacts between substrate/coenzyme and active site residues in both systems. The PsFDH system exhibits some additional hydrogen bonds between NADH and the enzyme that do not exist in the CbFDH system. This is due to the sequence differences between the two species. However, both systems show a similar hydrogen-bonding network in the active site with small distance variations between the phenotypes. Based on these results we conclude that these two FDHs have very similar reaction coordinate with similar transition states (identical to within accuracy of our methods), as well as similar active site structural features. Moreover, we conclude that both holo-enzyme crystal structures represent catalytically competent forms of the enzyme.

## CONCLUSIONS

We report the first ligand-bound, closed conformation, structure of CbFDH. In previous attempts to crystallize this enzyme, Schirwitz et al.[20] suggested that wild type CbFDH did not crystallize to well diffracting crystals because of a “surface-entropy shield”. They crystallized the apo-CbFDH and achieved good resolution diffraction data only by introducing surface mutations (e.g., K328V and K47E), designed for “entropy reducing site-directed mutagenesis”.[20] In the current study both apo- and holo-CbFDH were obtained without introducing any mutations. The recombinant CbFDH used by Schirwitz et al.[20] also possesses three natural hydrophobic variants at residues close to the homodimer interface, which might further destabilize that protein, relative to the isozyme reported here.

The fortuitous finding that the apo-CbFDH was also obtained from solution where it was a negligible fraction is intriguing. A kinetic explanation is proposed in Figure 3, where the formation of a nucleation center can lead to crystallization of apo-enzyme despite it being a negligible form in solution. From the examination of crystal packing, it appears that the apo- and holo-enzymes adopted different packing patterns between unit cells, and, once crystallized, inter-conversion between those structures is not possible. This finding raises the need to practice great caution when assuming that any crystal structure of a protein represents a dominant conformation in solution.

The new structure of the holo-CbFDH in complex with its co-factor ($NAD^+$) and TSA (azide) is of great interest for both basic studies of the enzyme functional dynamics and practical purposes related to its industrial uses. The first relates to CbFDH use as a model system to study the relation between protein dynamics at the fs to ps time scales and the catalyzed chemistry. Following those fast dynamics using 2D IR of the holo-enzyme to monitor the dynamic environment of the azide in the FDH-$NAD^+$-azide ternary complex can

now be compared to the catalyzed C-H bond activation (Scheme 1) examined by means of intrinsic KIE and its temperature dependence. The new structure now enables the design of mutants that will rigorously alter the DAD and its dynamics at the catalyzed transition state. Those mutants will be used to seek correlation between the reactive complex dynamics and catalysis. QM/MM free energy simulations examined the catalytic competency of the holo-CbFDH crystal structure, and we conclude that simulations commencing with the new structure yield a free energy profile in agreement with experimental estimates and that is very similar to the one obtained from holo-PsFDH. From a practical prospective, CbFDH is widely used in industry and structure-based mutagenesis has been attempted for different purposes,[72] and the new structural information may assist in the design of beneficial mutants.

## Supplementary Material

Refer to Web version on PubMed Central for supplementary material.

## Acknowledgments

We thank Dr. Nikolaos Labrou from Agricultural University of Athens for providing us the recombinant CbFDH plasmid.

**FUNDING INFORMATION**

This work was supported by grants from the NIH GM065368, the NSF CHE-1149023, and BSF 2012340 to AK and DTM, and GM079368 to CMC.

## ABBREVIATIONS

| | |
|---|---|
| **CbFDH** | *Candida boidinii* formate dehydrogenase |
| **PsFDH** | *Pseudomonas* sp. 101 formate dehydrogenase |
| **NAD** | nicotinamide adenine dinucleotide |
| **NADH** | reduced nicotinamide adenine dinucleotide |
| **DAD** | donor-acceptor distance |
| **TRS** | tunneling ready state |
| **fs** | femtosecond |
| **ps** | picosecond |
| **2D-IR** | two-dimensional infrared spectroscopy |
| **QM/MM** | quantum mechanical/molecular mechanical |
| **CPT** | constant pressure/temperature |
| **NOE** | nuclear Overhauser effect |
| **US** | umbrella sampling |

| | |
|---|---|
| **CM-PMF** | classical-mechanical potential of mean force |
| **WHAM** | weighted histogram analysis method |
| **TSA** | transition state analogue |

## References


1. Unden G, Kroger A. Reconstitution of a functional electron-transfer chain from purified formate dehydrogenase and fumarate reductase complexes. Methods Enzymol. 1986; 126:387–399. [PubMed: 2856137]
2. Bandaria JN, Cheatum CM, Kohen A. Examination of Enzymatic H-Tunneling through Kinetics and Dynamics. J Am Chem Soc. 2009; 131:10151–10155. [PubMed: 19621965]
3. Torres RA, Schiøtt B, Bruice TC. Molecular Dynamics Simulations of Ground and Transition States for the Hydride Transfer from Formate to NAD+ in the Active Site of Formate Dehydrogenase. J Am Chem Soc. 1999; 121:8164–8173.
4. Popov VO, Lamzin VS. NAD(+)-dependent formate dehydrogenase. Biochem J. 1994; 301:625–643. [PubMed: 8053888]
5. Blanchard JS, Cleland WW. Kinetic and chemical mechanisms of yeast formate dehydrogenase. Biochemistry. 1980; 19:3543–3550. [PubMed: 6996706]
6. Bandaria JN, Cheatum CM, Kohen A. Examination of Enzymatic H-Tunneling through Kinetics and Dynamics. J Am Chem Soc. 2009; 131:10151–10155. [PubMed: 19621965]
7. Dutta S, Li YL, Rock W, Houtman JCD, Kohen A, Cheatum CM. 3-Picolyl Azide Adenine Dinucleotide as a Probe of Femtosecond to Picosecond Enzyme Dynamics. J Phys Chem B. 2011; 116:542–548. [PubMed: 22126535]
8. Hill SE, Bandaria JN, Fox M, Vanderah E, Kohen A, Cheatum CM. Exploring the Molecular Origins of Protein Dynamics in the Active Site of Human Carbonic Anhydrase II. J Phys Chem B. 2009; 113:11505–11510. [PubMed: 19637848]
9. Thielges MC, Axup JY, Wong D, Lee HS, Chung JK, Schultz PG, Fayer MD. Two-Dimensional IR Spectroscopy of Protein Dynamics Using Two Vibrational Labels: A Site-Specific Genetically Encoded Unnatural Amino Acid and an Active Site Ligand. J Phys Chem B. 2011; 115:11294–11304. [PubMed: 21823631]
10. Bandaria JN, Dutta S, Hill SE, Kohen A, Cheatum CM. Fast Enzyme Dynamics at the Active Site of Formate Dehydrogenase. J Am Chem Soc. 2007; 130:22–23. [PubMed: 18067303]
11. Bandaria JN, Dutta S, Nydegger MW, Rock W, Kohen A, Cheatum CM. Characterizing the dynamics of functionally relevant complexes of formate dehydrogenase. Proc Natl Acad Sci U S A. 2010; 107:17974–17979. [PubMed: 20876138]
12. Stojković V, Perissinotti LL, Willmer D, Benkovic SJ, Kohen A. Effects of the Donor–Acceptor Distance and Dynamics on Hydride Tunneling in the Dihydrofolate Reductase Catalyzed Reaction. J Am Chem Soc. 2011; 134:1738–1745. [PubMed: 22171795]
13. Meyer MP, Tomchick DR, Klinman JP. Enzyme structure and dynamics affect hydrogen tunneling: The impact of a remote side chain (I553) in soybean lipoxygenase-1. Proc Natl Acad Sci U S A. 2008; 105:1146–1151. [PubMed: 18216254]
14. Bahnson BJ, Colby TD, Chin JK, Goldstein BM, Klinman JP. A link between protein structure and enzyme catalyzed hydrogen tunneling. Proc Natl Acad Sci U S A. 1997; 94:12797–12802. [PubMed: 9371755]
15. Kohen A. Role of Dynamics in Enzyme Catalysis: Substantial versus Semantic Controversies. Acc Chem Res. 2015; 48:466–473. [PubMed: 25539442]
16. Castillo R, Oliva M, Martí S, Moliner V. A Theoretical Study of the Catalytic Mechanism of Formate Dehydrogenase. J Phys Chem B. 2008; 112:10012–10022. [PubMed: 18646819]
17. Roca M, Oliva M, Castillo R, Moliner V, Tunon I. Do dynamic effects play a significant role in enzymatic catalysis? A theoretical analysis of formate dehydrogenase. Chem Eur J. 2010; 16:11399–11411. [PubMed: 20715198]

18. Vardi-Kilshtain A, Major DT, Kohen A, Engel H, Doron D. Hybrid Quantum and Classical Simulations of the Formate Dehydrogenase Catalyzed Hydride Transfer Reaction on an Accurate Semiempirical Potential Energy Surface. J Chem Theory Comput. 2012; 8:4786–4796. [PubMed: 26605631]
19. Nilov DK, Shabalin IG, Popov VO, Švedas VK. Molecular modeling of formate dehydrogenase: the formation of the Michaelis complex. J Biomol Struct Dyn. 2012; 30:170–179. [PubMed: 22702728]
20. Schirwitz K, Schmidt A, Lamzin VS. High-resolution structures of formate dehydrogenase from Candida boidinii. Protein Sci. 2007; 16:1146–1156. [PubMed: 17525463]
21. Kroner KH, Schütte H, Stach W, Kula MR. Scale-up of formate dehydrogenase by partition. J Chem Technol Biotechnol. 1982; 32:130–137.
22. Shaked, Ze; Whitesides, GM. Enzyme-catalyzed organic synthesis: NADH regeneration by using formate dehydrogenase. J Am Chem Soc. 1980; 102:7104–7105.
23. Wong CH, Whitesides GM. Enzyme-catalyzed organic synthesis: regeneration of deuterated nicotinamide cofactors for use in large-scale enzymatic synthesis of deuterated substances. J Am Chem Soc. 1983; 105:5012–5014.
24. Hatrongjit R, Packdibamrung K. A novel NADP+-dependent formate dehydrogenase from Burkholderia stabilis 15516: Screening, purification and characterization. Enzyme Microb Technol. 2010; 46:557–561.
25. Yadav RK, Baeg JO, Oh GH, Park NJ, Kong K-j, Kim J, Hwang DW, Biswas SK. A Photocatalyst–Enzyme Coupled Artificial Photosynthesis System for Solar Energy in Production of Formic Acid from CO2. J Am Chem Soc. 2012; 134:11455–11461. [PubMed: 22769600]
26. Labrou NE, Karagouni A, Clonis YD. Biomimetic-dye affinity adsorbents for enzyme purification: application to the one-step purification of Candida boidinii formate dehydrogenase. Biotechnol Bioeng. 1995; 48:278–288. [PubMed: 18623487]
27. Labrou NE. Improved purification of Candida boidinii formate dehydrogenase. Bioseparation. 2000; 9:99–104. [PubMed: 10892543]
28. Kabsch W. XDS. Acta Crystallogr Sect D: Biol Crystallogr. 2010; 66:125–132. [PubMed: 20124692]
29. McCoy AJ, Grosse-Kunstleve RW, Adams PD, Winn MD, Storoni LC, Read RJ. Phaser crystallographic software. J Appl Crystallogr. 2007; 40:658–674. [PubMed: 19461840]
30. Collaborative Computational Project, N. The CCP4 suite: programs for protein crystallography. Acta Crystallogr Sect D: Biol Crystallogr. 1994; 50:760–763. [PubMed: 15299374]
31. Emsley P, Cowtan K. Coot: model-building tools for molecular graphics. Acta Crystallogr Sect D: Biol Crystallogr. 2004; 60:2126–2132. [PubMed: 15572765]
32. Pannu NS, Murshudov GN, Dodson EJ, Read RJ. Incorporation of prior phase information strengthens maximum-likelihood structure refinement. Acta Crystallogr Sect D: Biol Crystallogr. 1998; 54:1285–1294. [PubMed: 10089505]
33. Romo, T.; Sacchettini, J.; Terwilliger, T.; Adams, P.; Afonine, P.; Grosse-Kunstleve, R.; Moriarty, N.; Sauter, N.; Zwart, P.; Gopal, K.; Ioerger, T.; Kanbi, L.; McKee, E.; Pai, R.; Hung, L-W.; Radhakannan, T.; McCoy, A.; Read, R.; Storoni, L. Automated structure determination with phenix. In: Read, R.; Sussman, J., editors. Evolving Methods for Macromolecular Crystallography. Springer; Netherlands: 2007. p. 101-109.
34. Cook, PF.; Cleland, WW. Enzyme Kinetics and Mechanism. Garland Publishing, Inc; New York, NY: 2007.
35. Quirk DJ, Northrop DB. Effect of Pressure on Deuterium Isotope Effects of Formate Dehydrogenase. Biochemistry. 2000; 40:847–851. [PubMed: 11170403]
36. Warshel A, Levitt M. Theoretical studies of enzymic reactions: Dielectric, electrostatic and steric stabilization of the carbonium ion in the reaction of lysozyme. J Mol Biol. 1976; 103:227–249. [PubMed: 985660]
37. Dewar MJS, Zoebisch EG, Healy EF, Stewart JJP. Development and use of quantum mechanical molecular models. 76. AM1: a new general purpose quantum mechanical molecular model. J Am Chem Soc. 1985; 107:3902–3909.

38. Rossi I, Truhlar DG. Parameterization of NDDO wavefunctions using genetic algorithms. An evolutionary approach to parameterizing potential energy surfaces and direct dynamics calculations for organic reactions. Chem Phys Lett. 1995; 233:231–236.
39. Jorgensen WL, Chandrasekhar J, Madura JD, Impey RW, Klein ML. Comparison of simple potential functions for simulating liquid water. J Chem Phys. 1983; 79:926–935.
40. MacKerell AD, Bashford D, Bellott M, Dunbrack RL, Evanseck JD, Field MJ, Fischer S, Gao J, Guo H, Ha S, Joseph-McCarthy D, Kuchnir L, Kuczera K, Lau FTK, Mattos C, Michnick S, Ngo T, Nguyen DT, Prodhom B, Reiher WE, Roux B, Schlenkrich M, Smith JC, Stote R, Straub J, Watanabe M, Wiórkiewicz-Kuczera J, Yin D, Karplus M. All-Atom Empirical Potential for Molecular Modeling and Dynamics Studies of Proteins. J Phys Chem B. 1998; 102:3586–3616. [PubMed: 24889800]
41. Nam K, Gao J, York DM. An Efficient Linear-Scaling Ewald Method for Long-Range Electrostatic Interactions in Combined QM/MM Calculations. J Chem Theory Comput. 2005; 1:2–13. [PubMed: 26641110]
42. Andersen HC. Molecular dynamics simulations at constant pressure and/or temperature. J Chem Phys. 1980; 72:2384–2393.
43. Hoover WG. Canonical dynamics: Equilibrium phase-space distributions. Phys Rev A. 1985; 31:1695–1697.
44. Hockney RW. Potential calculation and some applications. Methods Comput Phys. 1970; 9:135–211.
45. Ryckaert JP, Ciccotti G, Berendsen HJC. Numerical integration of the cartesian equations of motion of a system with constraints: molecular dynamics of n-alkanes. J Comput Phys. 1977; 23:327–341.
46. Brooks BR, Bruccoleri RE, Olafson BD, States DJ, Swaminathan S, Karplus M. CHARMM: A program for macromolecular energy, minimization, and dynamics calculations. J Comput Chem. 1983; 4:187–217.
47. Brooks BR, Brooks CL, Mackerell AD, Nilsson L, Petrella RJ, Roux B, Won Y, Archontis G, Bartels C, Boresch S, Caflisch A, Caves L, Cui Q, Dinner AR, Feig M, Fischer S, Gao J, Hodoscek M, Im W, Kuczera K, Lazaridis T, Ma J, Ovchinnikov V, Paci E, Pastor RW, Post CB, Pu JZ, Schaefer M, Tidor B, Venable RM, Woodcock HL, Wu X, Yang W, York DM, Karplus M. CHARMM: The biomolecular simulation program. J Comput Chem. 2009; 30:1545–1614. [PubMed: 19444816]
48. Torrie GM, Valleau JP. Nonphysical sampling distributions in Monte Carlo free-energy estimation: Umbrella sampling. J Comput Phys. 1977; 23:187–199.
49. Kumar S, Rosenberg JM, Bouzida D, Swendsen RH, Kollman PA. THE weighted histogram analysis method for free-energy calculations on biomolecules. I. The method. J Comput Chem. 1992; 13:1011–1021.
50. Robert X, Gouet P. Deciphering key features in protein structures with the new ENDscript server. Nucleic Acids Res. 2014; 42:W320–W324. [PubMed: 24753421]
51. Serov AE, Popova AS, Fedorchuk VV, Tishkov VI. Engineering of coenzyme specificity of formate dehydrogenase from Saccharomyces cerevisiae. Biochem J. 2002; 367:841–847. [PubMed: 12144528]
52. Cousido-Siah A, Petrova T, Hazemann I, Mitschler A, Ruiz FX, Howard E, Ginell S, Atmanene C, Van Dorsselaer A, Sanglier-Cianférani S, Joachimiak A, Podjarny A. Crystal packing modifies ligand binding affinity: The case of aldose reductase. Proteins: Struc Funct, Bioinf. 2012; 80:2552–2561.
53. Chen RQ, Lu QQ, Cheng QD, Ao LB, Zhang CY, Hou H, Liu YM, Li DW, Yin DC. An ignored variable: solution preparation temperature in protein crystallization. Sci Rep. 2015; 5:7797. [PubMed: 25597864]
54. Wang Z, Kohen A. Thymidylate Synthase Catalyzed H-Transfers: Two Chapters in One Tale. J Am Chem Soc. 2010; 132:9820–9825. [PubMed: 20575541]
55. Roston D, Kohen A. Elusive transition state of alcohol dehydrogenase unveiled. Proc Natl Acad Sci U S A. 2010; 107:9572–9577. [PubMed: 20457944]

56. Wang Z, Abeysinghe T, Finer-Moore JS, Stroud RM, Kohen A. A Remote Mutation Affects the Hydride Transfer by Disrupting Concerted Protein Motions in Thymidylate Synthase. J Am Chem Soc. 2012; 134:17722–17730. [PubMed: 23034004]
57. Wang Z, Sapienza PJ, Abeysinghe T, Luzum C, Lee AL, Finer-Moore JS, Stroud RM, Kohen A. Mg2+ Binds to the Surface of Thymidylate Synthase and Affects Hydride Transfer at the Interior Active Site. J Am Chem Soc. 2013; 135:7583–7592. [PubMed: 23611499]
58. Francis K, Stojkovic V, Kohen A. Preservation of protein dynamics in dihydrofolate reductase evolution. J Biol Chem. 2013; 288:35961–35968. [PubMed: 24158440]
59. Singh P, Sen A, Francis K, Kohen A. Extension and Limits of the Network of Coupled Motions Correlated to Hydride Transfer in Dihydrofolate Reductase. J Am Chem Soc. 2014; 136:2575–2582. [PubMed: 24450297]
60. Roston D, Islam Z, Kohen A. Kinetic isotope effects as a probe of hydrogen transfers to and from common enzymatic cofactors. Arch Biochem Biophys. 2014; 544:96–104. [PubMed: 24161942]
61. Sikorski RS, Wang L, Markham KA, Rajagopalan PTR, Benkovic SJ, Kohen A. Tunneling and Coupled Motion in the Escherichia coli Dihydrofolate Reductase Catalysis. J Am Chem Soc. 2004; 126:4778–4779. [PubMed: 15080672]
62. Hu S, Sharma SC, Scouras AD, Soudackov AV, Carr CA, Hammes-Schiffer S, Alber T, Klinman JP. Extremely elevated room-temperature kinetic isotope effects quantify the critical role of barrier width in enzymatic C-H activation. J Am Chem Soc. 2014; 136:8157–8160. [PubMed: 24884374]
63. Sharma SC, Klinman JP. Kinetic Detection of Orthogonal Protein and Chemical Coordinates in Enzyme Catalysis: Double Mutants of Soybean Lipoxygenase. Biochemistry. 2015; 54:5447–5456. [PubMed: 26154975]
64. Liang ZX, Lee T, Resing KA, Ahn NG, Klinman JP. Thermal-activated protein mobility and its correlation with catalysis in thermophilic alcohol dehydrogenase. Proc Natl Acad Sci U S A. 2004; 101:9556–9561. [PubMed: 15210941]
65. Nagel ZD, Cun S, Klinman JP. Identification of a long-range protein network that modulates active site dynamics in extremophilic alcohol dehydrogenases. J Biol Chem. 2013; 288:14087–14097. [PubMed: 23525111]
66. Garcia-Viloca M, Poulsen TD, Truhlar DG, Gao J. Sensitivity of molecular dynamics simulations to the choice of the X-ray structure used to model an enzymatic reaction. Prot Sci. 2004; 13:2341–2354.
67. Swiderek K, Kohen A, Moliner V. The influence of active site conformations on the hydride transfer step of the thymidylate synthase reaction mechanism. Phys Chem Chem Phys. 2015; 17:30793–30804. [PubMed: 25868526]
68. Major DT, Gao J. An Integrated Path Integral and Free-Energy Perturbation–Umbrella Sampling Method for Computing Kinetic Isotope Effects of Chemical Reactions in Solution and in Enzymes. J Chem Theory Comput. 2007; 3:949–960. [PubMed: 26627415]
69. Cao J, Voth GA. A unified framework for quantum activated rate processes. I. General theory. J Chem Phys. 1996; 105:6856–6870.
70. Gillan MJ. Quantum simulation of hydrogen in metals. Phys Rev Lett. 1987; 58:563–566. [PubMed: 10034973]
71. Tishkov VI, Popov VO. Catalytic mechanism and application of formate dehydrogenase. Biochemistry Biokhimiia. 2004; 69:1252–1267. [PubMed: 15627379]
72. Tishkov VI, Popov VO. Protein engineering of formate dehydrogenase. Biomolecular engineering. 2006; 23:89–110. [PubMed: 16546445]


**Figure 1.**

Sequence alignment generated by ESPript 3.0[50] between the wild type recombinant enzyme used here, CbFDH_iso2 (top), CbFDH_iso1 with K328V mutation (middle), and PsFDH (bottom). Red boxes with white characters denote strict identity, red characters denote similarity in a group and blue frame denotes similarity across groups. The dots above each aligned sequences mark every tenth residue (based on recombinant) to keep track of the sequence numbering. The non-conserved variants sites, L128, I227 and I354, are highlighted with blue *.

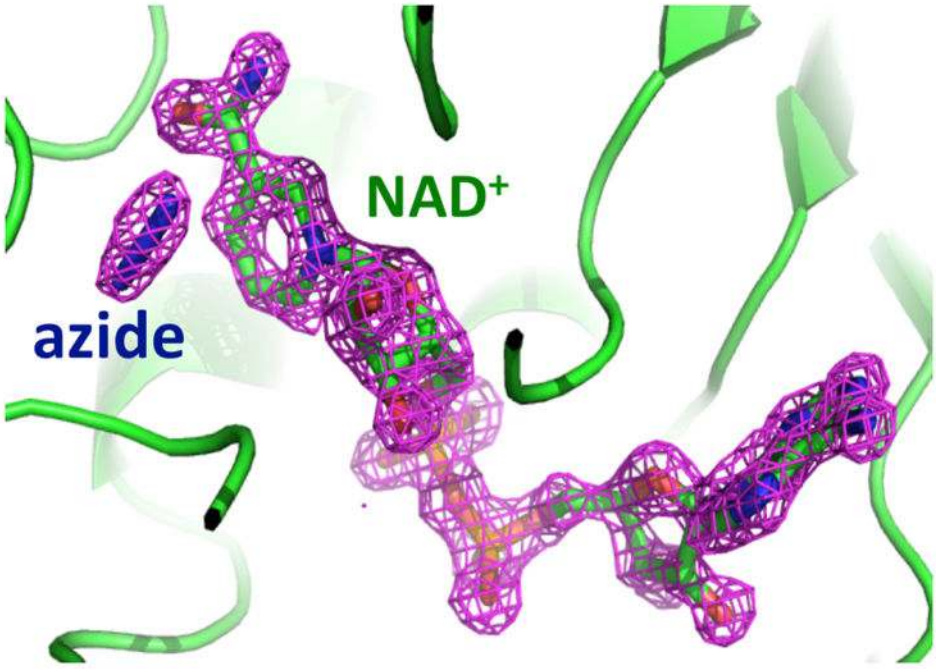


**Figure 2.**

Active site of holo-CbFDH (PDB ID 5DN9) with Fo-Fc map (magenta) for the two ligands (azide in blue and $NAD^+$ in green) calculated before the ligand was modeled in is shown contoured at 3σ and carved at 2 Å around the ligands.

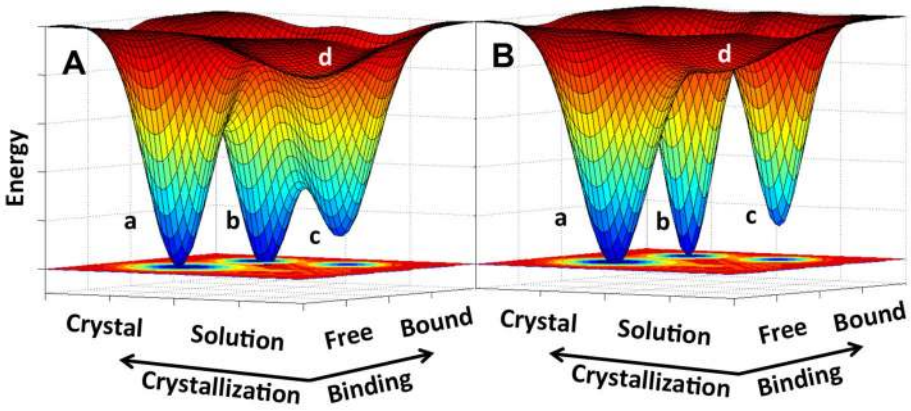


**Figure 3.**

Hypothetical potential energy surfaces for (A) initial nucleation that favors crystallization of holo-enzyme, and (B) initial nucleation that favors the free apo-enzyme. The marked minima are for apo-enzyme crystal (a), ternary complex crystal (b) enzymatic complex in solution (c) and free apo-enzyme in solution (d). The hypothesis behind this landscape is encapsulated in the low kinetic barrier between **c** and **b** states in A, and the lower barrier between **d** and **a** states in B.

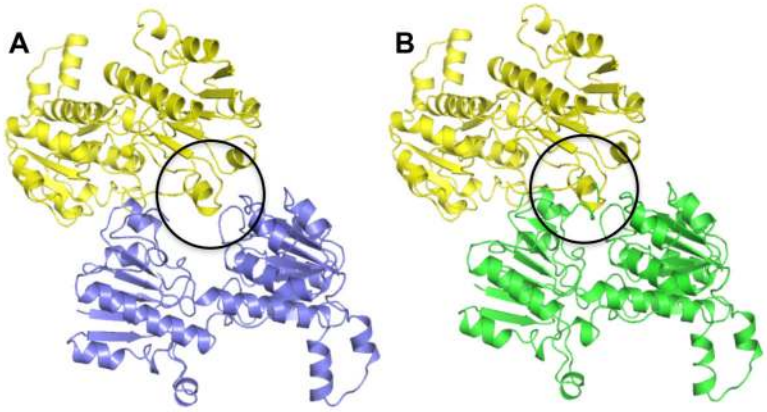


**Figure 4.**

Packing of apo- and holo-CbFDH. Panel A shows the apo-enzyme while emphasizing the packing between apo-CbFDH (PDB 5DNA) chain A (blue) and chain D (yellow) from a neighboring cell unit. Panel B shows the same asymmetric unit for the holo-CbFDH (green, PDB 5DN9). The region highlighted within the black circle shows the closed conformation of the holo-enzyme has more interaction surface with the neighboring unit than the open conformation of the apo-enzyme.

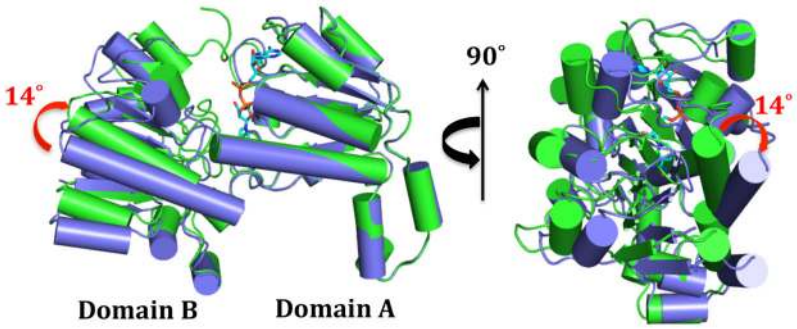


**Figure 5.**

Comparison of chain A between holo- (green, PDB 5DN9) to apo-CbFDH (blue, PDB 5DNA). To emphasize the needed relative motion between domains A and B when binding the ligands, the overlay was forced on domain A (residue 121–311). The angle was measured between the same α-helix (residue 318–337) from the two structures. The two panels present two different views of the overlaid structures.

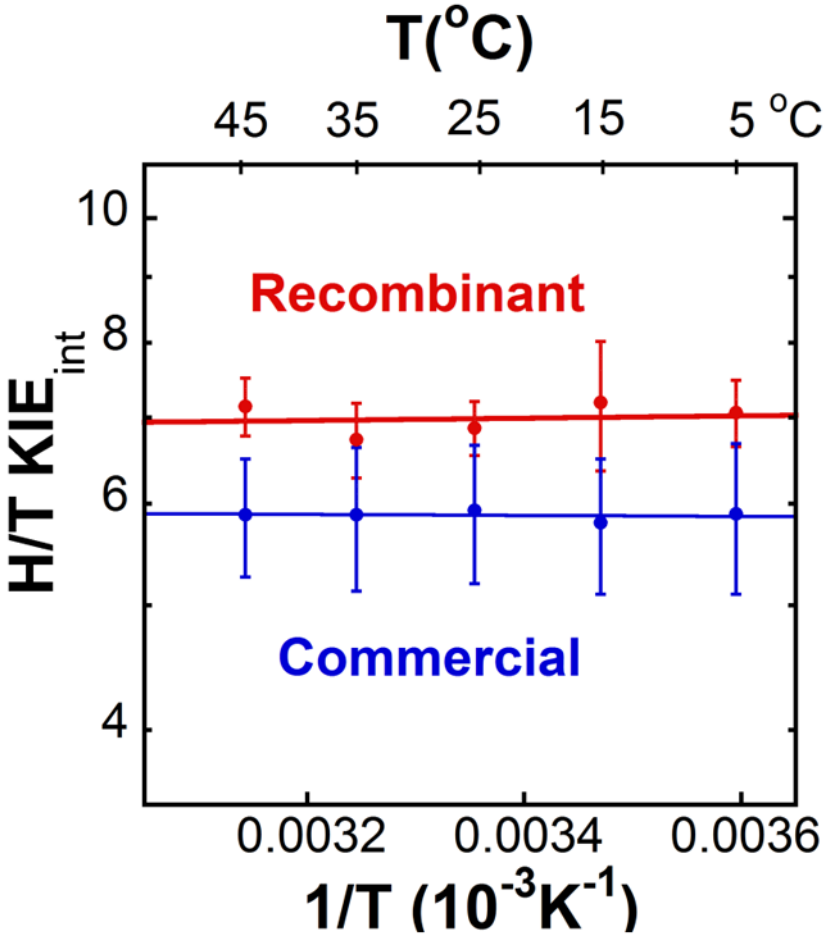


**Figure 6.**

Arrhenius plots of the intrinsic H/T KIEs (log scale) on the hydride transfer reaction catalyzed by recombinant (red) and commercial CbFDHs (blue). Average KIEs are presented as points with their standard deviations. The lines are non-linear fits of all the data points to the Arrhenius equation.

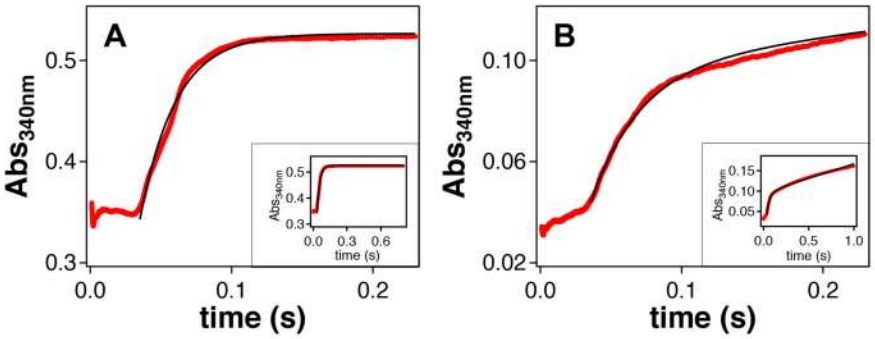


**Figure 7.**

Representative progress curves for the hydride transfer reaction catalyzed by recombinant (A) and commercial (B) CbFDH under single turnover conditions. The red traces represent the experimental data while the black lines are the fits of the data to either single exponential (A) or burst equation (B). Insets are the full progress curve from 0 – 1 sec.

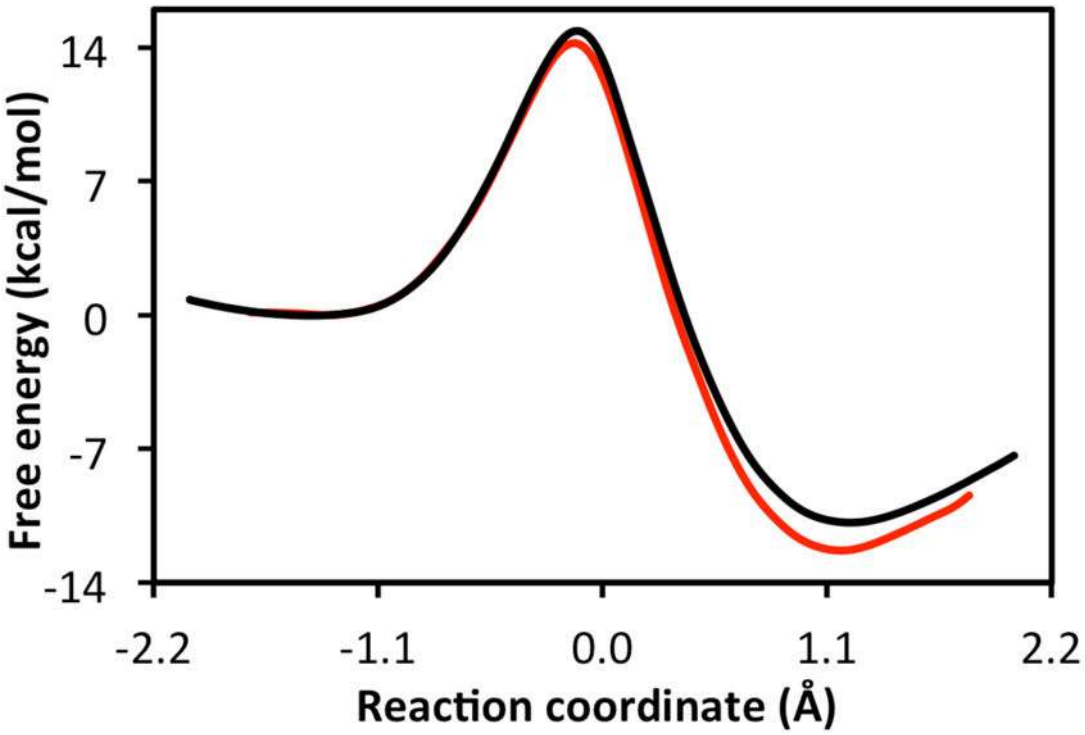


**Figure 8.**
Classical free energy profiles for PsFDH (black) and CbFDH (red).

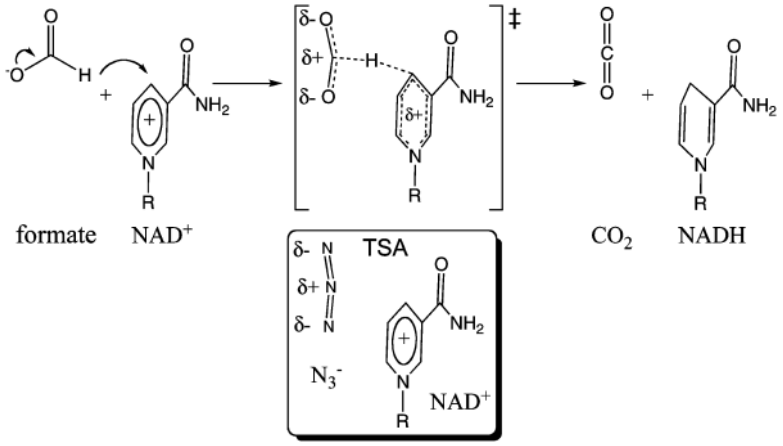


**Scheme 1.**

Hydride-transfer reaction catalyzed by FDH, with an illustration of the transition state structure (‡) and the transition state analogue (TSA) azide anion (reprinted from ref 6). Copyright (2009) American Chemical Society.

## Table 1

Comparison of the steady-state kinetic parameters for recombinant, K328V, commercial CbFDH and PsFDH

| | Recombinant | K328V[a] | Commercial[a] | PsFDH[b] |
|---|---|---|---|---|
| $k_{cat}$ ($s^{-1}$) | 5.6 ± 0.2 | 6.8 ± 0.3 | 4.9 ± 0.3 | 10.0 ± 0.6 |
| $K_{M/NAD+}$ (μM) | 30.3 ± 2.1 | 25.0 ± 1.3 | 50.0 ± 2.5 | 60 ± 5 |
| $k_{cat}/K_{M/NAD+}$ ($M^{-1}s^{-1}$) | (1.8 ± 0.1) x$10^5$ | (2.7 ± 0.2) x$10^5$ | (0.98 ±0.08) x$10^5$ | (1.7 ± 0.2) x$10^5$ |
| $K_{M/formate}$ (mM) | 4.0 ± 0.6 | 5.0 ± 0.3 | 20.0 ± 1.0 | 7.0 ± 0.8 |
| $k_{cat}/K_{M/formate}$ ($M^{-1}s^{-1}$) | (1.4 ± 0.2) x$10^3$ | (1.4 ± 0.1) x$10^3$ | (0.25 ± 0.02) x$10^3$ | (1.4 ± 0.2) x$10^3$ |

[a] From ref 20 and

[b] From ref 51.

**Table 2**

Free energies of reaction, $\Delta G_r$, and activation, $\Delta G‡$, (kcal/mol) calculated from classical (CM) and quantum mechanical (QM) potentials of mean force for the hydride transfer reaction in PsFDH and CbFDH based on the QM(AM1-SRP)/MM Hamiltonian.

| | $\Delta G^{‡}_{CM}$ | $\Delta G^{‡}_{QM}$ | $\Delta G_r$ |
|---|---|---|---|
| **PsFDH** | 14.9 | 13.0 | −10.8 |
| **CbFDH** | 14.2 | 12.2 | −12.3 |